Available online at www.sciencedirect.com
ScienceDirect
Journal of Sound and Vibration 315 (2008) 394–413
JOURNAL OF SOUND AND VIBRATION
www.elsevier.com/locate/jsvi

Space–time numerical simulation and validation of analytical predictions for nonlinear forced dynamics of suspended cables

Narakorn Srinil[a,*], Giuseppe Rega[b]

[a]Department of Engineering, University of Aberdeen, King's College, Aberdeen, AB24 3UE Scotland, UK
[b]Department of Structural and Geotechnical Engineering, SAPIENZA University of Rome, via A. Gramsci 53, Rome 00197, Italy

Accepted 19 December 2007
The peer review of this article was organised by the Guest Editor
Available online 8 February 2008

Abstract

This paper presents space–time numerical simulation and validation of analytical predictions for the finite-amplitude forced dynamics of suspended cables. The main goal is to complement analytical and numerical solutions, accomplishing overall quantitative/qualitative comparisons of nonlinear response characteristics. By relying on an approximate, kinematically non-condensed, planar modeling, a simply supported horizontal cable subject to a primary external resonance and a 1:1, or 1:1 vs. 2:1, internal resonance is analyzed. To obtain analytical solution, a second-order multiple scales approach is applied to a complete eigenfunction-based series of nonlinear ordinary-differential equations of cable damped forced motion. Accounting for both quadratic/cubic geometric nonlinearities and multiple modal contributions, local scenarios of cable uncoupled/coupled responses and associated stability are predicted, based on chosen reduced-order models. As a cross-checking tool, numerical simulation of the associated nonlinear partial–differential equations describing the dynamics of the actual infinite-dimensional system is carried out using a finite difference technique employing a hybrid explicit–implicit integration scheme. Based on system control parameters and initial conditions, cable amplitude, displacement and tension responses are numerically assessed, thoroughly validating the analytically predicted solutions as regards the actual existence, the meaningful role and the predominating internal resonance of coexisting/competing dynamics. Some methodological aspects are noticed, along with a discussion on the kinematically approximate versus exact, as well as planar versus non-planar, cable modeling.

1. Introduction

Numerous research contributions have witnessed a diverse interest in geometrically nonlinear dynamics of suspended cables, with several attempts to build a reliable theoretical framework for investigating such distributed-parameter systems with quadratic and cubic nonlinearities [1]. As closed-form exact solutions capturing the actual nonlinear dynamics cannot be sought for, most of the analytical investigations have been accomplished based on some a priori hypotheses concerned with the elasto-geometrical and kinematic modeling, the mechanical equations of motion, the spatial or temporal dependence of dynamical solutions,

*Corresponding author.
E-mail addresses: narakorn.srini@abdn.ac.uk (N. Srinil), giuseppe.rega@uniroma1.it (G. Rega).

0022-460X/$ - see front matter © 2007 Elsevier Ltd. All rights reserved.
doi:10.1016/j.jsv.2007.12.026

and the initial phase-space conditions leading to particular attractors. For qualifying the richness and variability of cable nonlinear dynamic characteristics under different external and/or internal resonances, a perturbation-based multiple scales (MS) approach has largely been applied to a crudely or properly reduced set of ordinary-differential equations (ODEs) of motion [2–9] or to an original system of partial-differential equations (PDEs) [2–6].

To avoid some or nearly all of the aforesaid hypotheses, computational treatments of the approximate [7,8] or exact [10,11] PDEs of cable motion have recently been accomplished based on a space–time finite-difference (FD) procedure confronting the finite-amplitude free vibration problems of sagged and arbitrarily inclined cables with/without internal resonances. In the meantime, several FD-based implementations have been used successfully to deal with a range of problems in nonlinear forced vibrations, including cables subject to random excitation [12], highly extensible cable mechanics [13], low-tension cables with large displacements [14] or semi-active vibration control strategies [15]. In aforesaid studies, the robustness, utility and versatility of FD algorithms have been evidenced.

However, as far as nonlinear dynamics of infinite-dimensional systems are concerned, little attention has been paid to validating the analytical predictions of ODEs via numerical simulation of PDEs. Yet, this is a crucial aspect from both a theoretical and a practical point of view because, when the system involves a large set of parameters due to, e.g., an internal resonance condition, the analytical approaches often fail to capture essential features of actual nonlinear dynamics, owing to the low-dimensional framework and several constraining assumptions. On the other hand, in addition to the prohibitive calculation costs, the accuracy of numerical simulation may be occasionally questionable for multi-degree-of freedom systems, particularly in the applications where space–time-varying behaviors are not easily traced out. Thus, both analytical and numerical solutions are of mutual significance, and relying upon solely one of them may entail incomplete or unreliable knowledge of system responses.

Abhyankar et al. [16] analyzed simply supported beams subject to a sinusoidal loading and showed a favorable comparison of chaotic responses between numerical FD (PDEs) and analytical (ODEs) solutions. Essebier and Baker [17] used spatial FDs and Runge–Kutta time integration of the ensuing ODEs to obtain undamped forced/unforced flexural responses against known analytical solutions of cantilever beams. For Euler–Bernoulli beams resting on a nonlinear elastic foundation and subject to primary/sub-harmonic resonances, Abe [18] showed that the shooting analysis of ODEs is superior to the MS analysis of the associated PDEs, in comparison with the FD analysis of PDEs. As far as cable nonlinear oscillations are concerned, Gattulli et al. [19] used analytical and finite element discretized models of ODEs to show some superior ability of the latter in capturing higher modal contributions. In turn, based on PDEs governing undamped unforced planar vibration, Srinil and Rega [8] have numerically checked the validity of some analytical reduced-order models for various horizontal/inclined sagged cables.

This paper aims to systematically and thoroughly compare numerical simulations and analytical predictions for nonlinear forced dynamics of suspended cables. The main goal is to complement analytical/numerical solutions, achieving overall quantitative and qualitative comparisons of the associated response characteristics. In this framework, to reduce the analytical/computational effort, reference is made to the simpler 2-D cable model, well knowing how this can be questionable to the aim of adequately describing the overall 3-D response scenario (see Section 4.3 forward). The paper is organized as follows. In Section 2, approximate nonlinear PDEs vs. ODEs of planar motion of a simply supported suspended cable subject to primary external and 1:1 or 2:1 internal resonance are summarized. Analytical and numerical solutions of ODEs and PDEs based on MS and FD methods, respectively, are presented. By focusing on horizontal cables at so-called crossovers in the natural frequency spectrum [20], Section 3 shows the analytical predictions provided by properly reduced-order models [8,9], by means of frequency-response curves. The influence of several control parameters is illustrated. Depending on response amplitudes, spatial nonlinear uncoupled/coupled dynamic configurations are analytically constructed and further utilized as displacement initiations in Section 4, where FD simulations of PDEs are performed, determining steady-state, multi-degree-of-freedom, responses. Various cases of 1:1, or 1:1 vs. 2:1, resonant modal interactions are numerically investigated to validate the analytical methodology and the outcomes, as well as the consequences of the approximate cable planar modeling. Section 5 summarizes the analyses and concludes the paper.

2. Cable model and solution methods

Let us consider nonlinear planar damped forced vibrations of a simply supported horizontal cable subject to a uniformly distributed vertical harmonic excitation (Fig. 1a). It is assumed that such continuous cable is linear elastic, and has moderate (low) dynamic (static) extensibility, negligible torsional, bending and shear rigidities. In a Cartesian X–Y coordinate frame, the small-sagged static equilibrium $y(x)$ under gravity g force is suitably described by a parabola [20], around which the cable oscillates with synchronous longitudinal $u(x,t)$ and vertical $v(x,t)$ displacements, $x(t)$ being the spatial (temporal) independent variable. In the following, the space-related (time-related) variables are non-dimensionalized with respect to cable span X_H $\left(X_H\sqrt{w_C/gH}\right)$, with H being the horizontal component of cable static tension and w_C the self-weight per unit unstretched length. A prime (dot) represents partial differentiation with respect to non-dimensional position (time).

2.1. Nonlinear partial/ordinary-differential equations of motion

With homogeneous boundary conditions, $u(0,\ t)=u(1,\ t)=v(0,\ t)=v(1,\ t)=0$, the approximate third-order PDEs governing the moderately large, damped, forced planar vibration of a suspended cable about its static equilibrium, in non-dimensional form, read [9]

$$\rho\ddot{u}+c\rho\dot{u}=\left\{u'+\frac{\alpha}{\rho^3}(u'+y'v')+\frac{\alpha}{\rho^3}\left(u'^2+y'u'v'+\frac{1}{2}\left(u'^2+v'^2\right)\right)+\frac{\alpha}{2\rho^3}\left(u'^3+u'v'^2\right)\right\}', \tag{1}$$

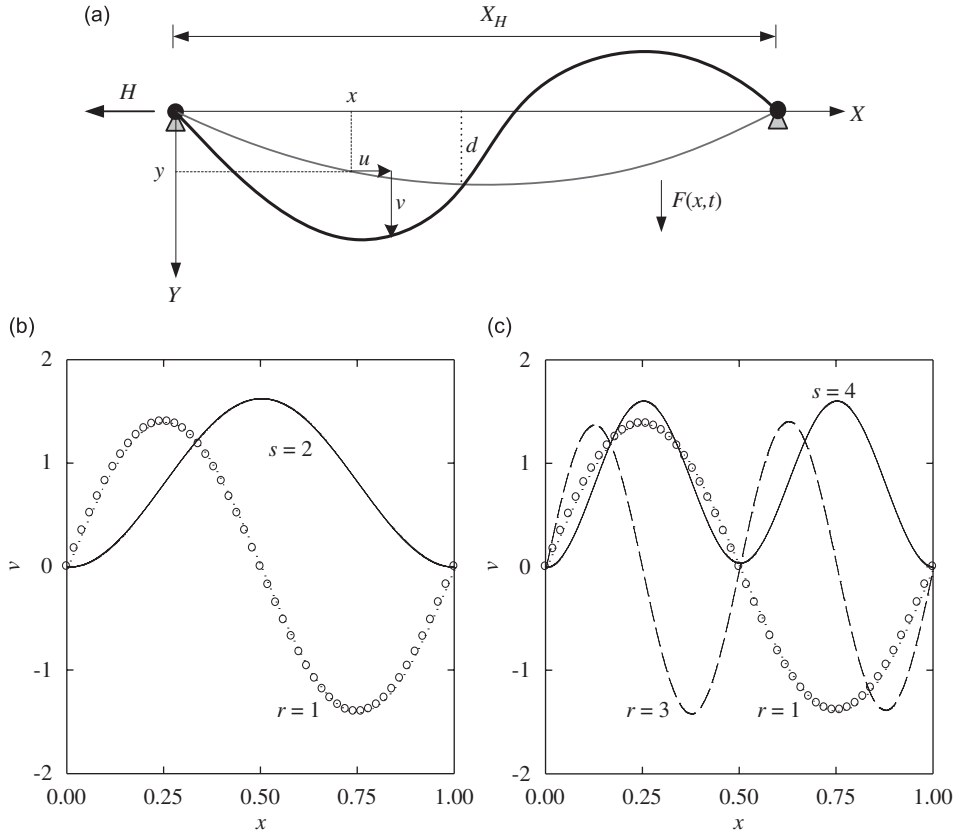

Fig. 1. Schematic suspended cable model (a) and orthonormalized v components of the eigenfunctions of resonant symmetric/anti-symmetric (s/r) modes at first (b) and second (c) crossovers.

$$\rho\ddot{v}+c\rho\dot{v}=\left\{v'+\frac{\alpha}{\rho^3}\left(y'u'+y'^2v'\right)+\frac{\alpha}{\rho^3}\left(u'v'+y'v'^2+\frac{y'}{2}\left(u'^2+v'^2\right)\right)+\frac{\alpha}{2\rho^3}\left(u'^2v'+v'^3\right)\right\}'+F\rho\cos\Omega t, \tag{2}$$

where $\rho=\left(1+y'^2\right)^{1/2}$, $\alpha=EA/H$, with EA being the cable axial stiffness, c the viscous damping coefficient, and F (Ω) the variable amplitude (frequency) of harmonic excitation.

Eqs. (1) and (2) couple both u and v dynamics with parabolic equilibrium, i.e., $y=4dx(1-x)$, in which d is the cable sag-to-span ratio [20], capture geometrically quadratic/cubic nonlinearities due to cable initial curvature and axial deformation, and are valid for both (zero sag) strings and arbitrarily inclined (asymmetric) cables [21]. It is necessary emphasizing that, in contrast with the unique integro-PDE of v motion typically considered in cable literature based on the quasi-static stretching assumption [1–6], this kinematically non-condensed system explicitly accounts for the longitudinal inertia and the space/time-varying dynamic tension [9]. To be generic, we keep herein exact ρ values throughout Eqs. (1) and (2) in the subsequent analyses, whereas $\rho\approx1$ in the associated linear terms in Ref. [9].

Casting Eqs. (1) and (2) in state-space form and using the orthonormality properties of linear eigenfunctions, the derived equations are then projected onto a full eigenspectrum by letting $U^J=\sum_{m=1}^{\infty}f_m\zeta_m^J$, $V^J=\sum_{m=1}^{\infty}p_m\zeta_m^J$, $J=1$–2, $U^1=u$, $U^2=v$, $V^1=\dot{u}$, $V^2=\dot{v}$, $\zeta_m^1=\phi_m$, $\zeta_m^2=\varphi_m$ with f_m (p_m) being the unknown displacement (velocity) coordinates of both u (ϕ_m) and v (φ_m) shape functions of the m mode of frequency ω_m, obtained via a sine-based series [7]. The Galerkin projection is applied, thereby giving rise to a complete infinite-dimensional set of ODEs

$$\begin{aligned}&\dot{f}_m-p_m=0,\\&\dot{p}_m+2\mu_mp_m+\omega_m^2f_m=\sum_{i=1}^{\infty}\sum_{j=1}^{\infty}\Lambda_{mij}f_if_j+\sum_{i=1}^{\infty}\sum_{j=1}^{\infty}\sum_{k=1}^{\infty}\Gamma_{mijk}f_if_jf_k+Z_m\cos\Omega t,\end{aligned} \tag{3}$$

for $m=1,\ 2,\ldots,\ \infty$, wherein $2\mu_m=c\int_0^1\rho\left(\phi_m^2+\varphi_m^2\right)\mathrm{d}x$ and $Z_m=F\int_0^1\rho\varphi_m\,\mathrm{d}x$ are modal damping and forcing terms. Expressions of the quadratic (Λ_{mij}) and cubic (Γ_{mijk}) nonlinear coefficients, accounting for the overall u and v modal shape contributions, can be found in Ref. [9]. In the following, we summarize the analytical MS solution for the nonlinear temporal behavior of ODEs (3), along with the numerical FD solution directly attacking the PDEs (Eqs. (1) and (2)).

2.2. Multiple scales solution with external/internal resonances

We pay our attention to planar internal resonances at meaningful crossovers [20]. To also highlight the influence of cable sag—as well as different features of mixed modal interactions—both first- and second-crossover horizontal cables are considered, the former exhibiting 1:1 resonance of first-symmetric/anti-symmetric modes, whereas the latter exhibiting 1:1 (2:1) resonance of second symmetric/anti-symmetric (second symmetric/first anti-symmetric) modes. To determine weakly nonlinear periodic responses and the associated local stability, Eq. (3) is analyzed based on a second-order MS approach capturing the slow variation of amplitudes and phases of uncoupled/coupled responses due to quadratic and cubic nonlinearities, damping and external/internal resonance [9]. With ε denoting a small bookkeeping parameter (which is finally taken as 1), the damping μ_m and excitation Z_m amplitudes are ordered such that they appear at the same ε^3 order, i.e., $\mu_m\to\varepsilon^2\mu_m$ and $Z_m\to\varepsilon^3Z_m$ in all resonance cases. In particular, the symmetric (s) mode is the directly excited mode with $Z_s\neq0$, whereas the corresponding anti-symmetric (r) mode is the internally resonant driven mode. The relationships of primary external and 1:1 internal resonances are quantified through $\Omega=\omega_s+\varepsilon^2\sigma_f$, $\omega_s=\omega_r+\varepsilon^2\sigma$, whereas those of primary external and 2:1 internal resonances read $\Omega=\omega_s+\varepsilon\sigma_f$, $\omega_s=2\omega_r+\varepsilon\sigma$, with σ_f and σ being external and internal detuning parameters, respectively.

The general approximate closed-form second-order solution of coupled forced damped dynamic configurations associated with both the u ($J=1$) and v ($J=2$) components for a 1:1 and 2:1 internally

resonant cable is expressed, respectively, as [9]

$$U^J(x,t) \approx a_r \cos(\Omega t-\gamma_r)\zeta_r^J(x)+a_s \cos(\Omega t-\gamma_s)\zeta_s^J(x) +\frac{1}{2}\{a_s^2[\cos(2\Omega t-2\gamma_s)\psi_{ss}^J(x)+\kappa_{ss}^J(x)]+a_r^2[\cos(2\Omega t-2\gamma_r)\psi_{rr}^J(x)+\kappa_{rr}^J(x)] +a_sa_r[\cos(2\Omega t-\gamma_r-\gamma_s)\psi_{rs}^J(x)+\cos(\gamma_r-\gamma_s)\kappa_{rs}^J(x)]\}, \tag{4}$$

$$U^J(x,t) \approx a_r \cos\left(\frac{\Omega t}{2}-\frac{\gamma_s}{2}-\frac{\gamma_r}{2}\right)\zeta_r^J(x)+a_s \cos(\Omega t-\gamma_s)\zeta_s^J(x) +\frac{1}{2}\left\{a_s^2[\cos(2\Omega t-2\gamma_s)\psi_{ss}^J(x)+\kappa_{ss}^J(x)]+a_r^2[\cos(\Omega t-\gamma_s-\gamma_r)\psi_{rr}^J(x)+\kappa_{rr}^J(x)] +a_sa_r\left[\cos\left(\frac{3}{2}\Omega t-\frac{3}{2}\gamma_s-\frac{1}{2}\gamma_r\right)\psi_{rs}^J(x)+\cos\left(\frac{1}{2}\Omega t-\frac{1}{2}\gamma_s+\frac{1}{2}\gamma_r\right)\kappa_{rs}^J(x)\right]\right\}. \tag{5}$$

Here, $\gamma_r=(\sigma_f+\sigma)t-\beta_r$, $\gamma_s=\sigma_f t-\beta_s$ in Eq. (4), whereas $\gamma_r=\sigma t-2\beta_r+\beta_s$, $\gamma_s=\sigma_f t-\beta_s$ in Eq. (5), with β_r (β_s) being the phase of the associated amplitude a_r (a_s). In addition to the first-order superimposition of resonant (ζ_r^J,ζ_s^J) modal functions with their correlated phases (e.g., Fig. 1b and c), the spatial displacement distributions in both Eqs. (4) and (5) further depend on second-order shape functions assembling the quadratic nonlinear effects of every retained resonant/non-resonant mode via $\psi_{ij}^J,\kappa_{ij}^J$ [6]. Similarly, second-order uncoupled dynamic configurations due to the solely primary resonance of symmetric mode can be extracted from Eq. (4) or (5). Meaningful temporal dependence and variation of second-order uncoupled (a_s) and coupled (a_r–a_s) amplitudes plus their relative phases (γ_r, γ_s) are enforced through the ensuing four-dimensional modulation equations [9], viz., for a 1:1 resonant modal interaction

$$\dot{a}_r=-\mu_r a_r+\frac{Ka_s^2a_r\sin(2\gamma_r-2\gamma_s)}{8\omega_r}, \tag{6}$$

$$a_r\dot{\gamma}_r=(\sigma_f+\sigma)a_r+\frac{K_{rr}a_r^3}{8\omega_r}+\frac{K_{rs}a_ra_s^2}{8\omega_r}+\frac{Ka_s^2a_r\cos(2\gamma_r-2\gamma_s)}{8\omega_r}, \tag{7}$$

$$\dot{a}_s=-\mu_s a_s-\frac{Ka_r^2a_s\sin(2\gamma_r-2\gamma_s)}{8\omega_s}+\frac{Z_s\sin\gamma_s}{2\omega_s}, \tag{8}$$

$$a_s\dot{\gamma}_s=\sigma_f a_s+\frac{K_{ss}a_s^3}{8\omega_s}+\frac{K_{rs}a_sa_r^2}{8\omega_s}+\frac{Ka_r^2a_s\cos(2\gamma_r-2\gamma_s)}{8\omega_s}+\frac{Z_s\cos\gamma_s}{2\omega_s}, \tag{9}$$

whereas for a 2:1 resonant modal interaction

$$\dot{a}_r=-\mu_r a_r+\frac{\Re a_ra_s\sin\gamma_r}{4\omega_r}, \tag{10}$$

$$a_r(\dot{\gamma}_r+\dot{\gamma}_s)=(\sigma_f+\sigma)a_r+\frac{\Re a_ra_s\cos\gamma_r}{2\omega_r}+\frac{K_{rr}a_r^3}{4\omega_r}+\frac{K_{rs}a_ra_s^2}{4\omega_r}, \tag{11}$$

$$\dot{a}_s=-\mu_s a_s-\frac{\Re a_r^2\sin\gamma_r}{8\omega_s}+\frac{Z_s\sin\gamma_s}{2\omega_s}, \tag{12}$$

$$a_s\dot{\gamma}_s=\sigma_f a_s+\frac{\Re a_r^2\cos\gamma_r}{8\omega_s}+\frac{K_{ss}a_s^3}{8\omega_s}+\frac{K_{rs}a_sa_r^2}{8\omega_s}+\frac{Z_s\cos\gamma_s}{2\omega_s}. \tag{13}$$

As discussed in Refs. [6–9], the non-trivial coefficient K or $\Re$ entails relevant 1:1 or 2:1 resonance activation because of the vanishing nonlinear orthogonality properties of resonant modes. Depending on control parameters, (σ,σ_f,μ,F), both Eqs. (6)–(9) and Eqs. (10)–(13) admit both uncoupled and coupled fixed-point ($\dot{a}_r=\dot{a}_s=\dot{\gamma}_r=\dot{\gamma}_s=0$) solutions. Relevant expressions of coefficients (K, $\Re$, K_{rr}, K_{ss}, K_{rs})—accounting for

quadratic/cubic nonlinearities and infinite-dimensional modal contributions—can be found in Ref. [9] along with comprehensive convergence analyses establishing properly reduced-order models.

2.3. Space–time finite-difference solution

Numerical simulation of the non-dimensional PDEs (1) and (2) governing the cable damped, forced, resonant motion is carried out by employing a second-order FD approach centrally approximating both spatial and temporal derivatives, thanks to a relevant straightforward routine developed by the authors in Refs. [10,11] to handle cable large-amplitude 3-D free vibrations. For the considered 2-D vibration problem, the continuous cable is divided into N equal space segments, which entails solving simultaneously a $2(N-1)$ multi-degree-of-freedom system for nonlinearly coupled u and v nodal components. Partitioning the time into a series of incremental steps, a hybrid explicit–implicit numerical integration scheme is adopted via a predictor–corrector iterative procedure and a specified tolerance controlling the global solution convergence at each time step. Due to the explicit–implicit implementation, it is generally true that the numerical simulation is stable if a sufficiently small time step is assigned [22,23].

As far as the initial state-space conditions are concerned, we assign zero velocities, but different spatial displacement configurations. In so doing, we utilize the known MS-based spatial distributions of uncoupled/coupled displacements (Eqs. (4) or (5)). Apart from establishing a link between numerical and analytical solutions, this allows us to determine (i) how nonlinear spatial MS solutions actually evolve with time and (ii) how much computational effort is needed in reaching a steady-state time response of a discretized, multi-degree-of-freedom system, with respect to the conventional zero initiation (i.e., cable at rest). Considering the same control parameters, it further allows us (iii) to validate the MS predictions against FD space–time laws with regard to the chosen reduced-order model embedded in the amplitude and displacement solutions (Eqs. (4)–(13)) [9], to the actual existence and role of stable/unstable, uncoupled/coupled, 1:1/2:1 resonant, equilibrium/periodic (constant/varying-amplitude) motion, and to the validity of asymptotic MS solutions when considering greater response amplitudes. Moreover, (iv) insightful multi-degree-of-freedom spatial comparison of MS vs. FD maximum dynamic displacements is of practical interest for accurate dynamic tension estimation, by also accounting for the approximate vs. exact [11] kinematically non-condensed modeling.

3. Analytical predictions via chosen reduced-order models

By considering the same cable properties as in Refs. [7–9], the elasto-geometric ($\alpha = EA/H$, d) dimensionless parameters of first- and second-crossover cables are ($\alpha = 642.72$, $d = 0.031$) and ($\alpha = 1024.28$, $d = 0.050$), respectively. The first-crossover cable exhibits (nearly tuned) 1:1 internal resonance, with $\omega_{s=2} \approx 6.287$ and $\omega_{r=1} \approx 6.252$, whereas the second-crossover cable exhibits either (nearly tuned) 1:1 or 2:1 internal resonance, with $\omega_{s=4} \approx 12.503$ and $\omega_{r=3} \approx 12.498$ or $\omega_{s=4}$ and $\omega_{r=1} \approx 6.205$, with the prevailing v component of the relevant linear orthonormalized (r, s) shape functions being displayed in Fig. 1b and c, respectively. As regards reduced-order models of amplitude/displacement solutions, a series of modal contribution and convergence analyses of second-order quadratic coefficients has been conducted as in Refs. [8,9]. For crossover cables, one may omit a priori negligible contributions of anti-symmetric non-resonant modes, whereas meaningful contributions of symmetric non-resonant modes should be accounted for along with those of the two resonant modes [9]. Accordingly, with M being the highest order of retained modes through overall coefficients in Eqs. (4)–(13), we have chosen $M = 10$ (without non-resonant anti-symmetric modes) for the first-crossover cable and $M = 15$ (with all modes, to possibly account for also a multiple internal resonance [9]) for the second-crossover cable.

3.1. Frequency-response diagrams and influence of control parameters

Based on the Cartesian version of modulation Eqs. (6)–(9) or (10)–(13), a series of frequency-response diagrams, whose bifurcations discriminate coupled from uncoupled (as well as fixed point from limit cycle) solution, is parametrically obtained via a continuation approach [24], which has been verified by a

Runge–Kutta time integration solution [9,21,25]. For the sake of ease, in the FD simulation of each resonance case (Section 4) we assume the modal damping $\mu = \mu_r = \mu_s$ (i.e., $2\mu_m \approx c$ due to the orthonormality condition of the modal integral part), because the corresponding damping coefficient c is a single input parameter in the PDEs (1) and (2). In the following, solid lines denote stable fixed points, whereas dashed (dotted) lines denote unstable fixed points settled down through saddle-node (SN) or pitchfork (PF) (Hopf) bifurcations.

The first-crossover cable involving 1:1 internal resonance is first analyzed. Three different cases—which assume perfect tuning of resonant frequencies, i.e., $\sigma = 0$—are considered, viz., (i) $\mu = 0.005$, $F = 0.005$, (ii) $\mu = 0.05$, $F = 0.005$, (iii) $\mu = 0.005$, $F = 0.010$, in order to examine the effect of varying damping (ii) or forcing (iii) parameter with respect to the reference (i) case. Associated frequency-response curves of coupled a_r (internally driven) and a_s (externally excited), and uncoupled a_s are plotted in Fig. 2a–c, respectively. To ascertain the possible σ effect, continuation of the (ii) case is also made with actual—albeit small—value of σ ($\omega_s - \omega_r \approx 0.005$), and only the coupled a_r–a_s results are traced out in Fig. 2a and b. Depending on the relative contributions of quadratic/cubic nonlinearities, overall frequency sweeping analyses in Fig. 2 highlight how the unstable coupled a_s branches (Fig. 2b) emanate from the uncoupled a_s ones (Fig. 2c) via double PF_1 and PF_2 bifurcations. Hysteresis (jump) phenomena are found in all uncoupled (Fig. 2c) and coupled (Fig. 2a and b) branches with multiple SN bifurcations, and the leaning-backbone softening behavior due to predominant quadratic nonlinearities is manifested (Fig. 2c).

Due to the activation of 1:1 internal resonance, stable (as well as unstable) coupled a_r and a_s occur over a wide σ_f range (Fig. 2a and b), with a_r (a_s) prevailing right (left) of the case of perfect primary resonance ($\sigma_f = 0$). It should also be noted that right (left) of the PF_2 (PF_1) bifurcation, the uncoupled (coupled) a_s values are greater than the corresponding coupled (uncoupled) a_s ones [9], and there is a range, bounded by PF_1 and PF_2 bifurcations, where only stable coupled a_r–a_s solutions exist, the larger (smaller) the F (μ) the greater the ensuing region. For the weaker-damped cases (i) and (iii), a marginal range (A or B) between Hopf bifurcations to which limit cycles are amenable is observed, being enlarged with increasing F. By increasing the damping by an order of magnitude ($\mu = 0.05$), i.e., case (ii) vs. (i), both amplitude responses and modal interaction effect are reduced due to a greater energy dissipation. In turn, considering the actual $\sigma = 0.005$ value quantitatively—though slightly—influences the driven a_r, rather than the excited a_s, with respect to the associated case (ii) with $\sigma = 0$. Yet, overall qualitative features practically remain the same in both σ cases, with a slight shift of SN and PF bifurcations. Accordingly, it appears sufficient to consider $\sigma = 0$ in the analytical solution.

Modal interactions in the second-crossover cable are now discussed in Fig. 3. By assigning the same parameters $\sigma = 0$, $\mu = 0.005$, $F = 0.005$ as in case (i) of first-crossover cable (Fig. 2), coupled a_r and a_s responses due to 1:1 or 2:1 resonance are independently traced out; they are then displayed altogether in Fig. 3a and b, respectively. The trend of both response curves qualitatively resembles that in Fig. 2: the coupled branches originate from the associated uncoupled ones (not shown), with PF, SN and Hopf (region C or D) bifurcations occurring at certain σ_f. However, here, both 1:1 and 2:1 resonant interactions persist throughout the considered σ_f range. The predominant role is played by either the driven a_r or the excited a_s in 1:1 resonant responses, depending on the sweeping σ_f parameter as in Fig. 2, whereas the driven a_r substantially prevails over the excited a_s in 2:1 resonant responses, regardless of σ_f. This means that the a_r mode behaves as an absorber with respect to the a_s mode, the energy being transferred from the latter to the former owing to 2:1 resonance. Such circumstance will be justified via numerical analyses in Section 4, along with the actual predominant role played by 2:1 vs. 1:1 resonant interactions and the validity of $\sigma = 0$ assumption.

3.2. Mixed/symmetric nonlinear dynamic displacements

By focusing on stable uncoupled/coupled solutions (Fig. 2 or 3), the corresponding nonlinear u and v displacements can be analytically constructed through Eq. (4) or (5). As FD simulations and spatial MS–FD displacement comparisons in Section 4 involve a multiple-dimensional phase-space spanned with u and v amplitudes (as well as their velocities) of every cable nodal vector, it is worth examining the spatio-temporal varying displacements of the cable when one of its nodal—essentially the prevailing v—components, contributing meaningfully to both uncoupled and coupled displacements, reaches its maximal amplitude either in the downward (Y^+) or upward (Y^-) direction (Fig. 1a). The cable mid-span ($x = 0.5$) or quarter-span from

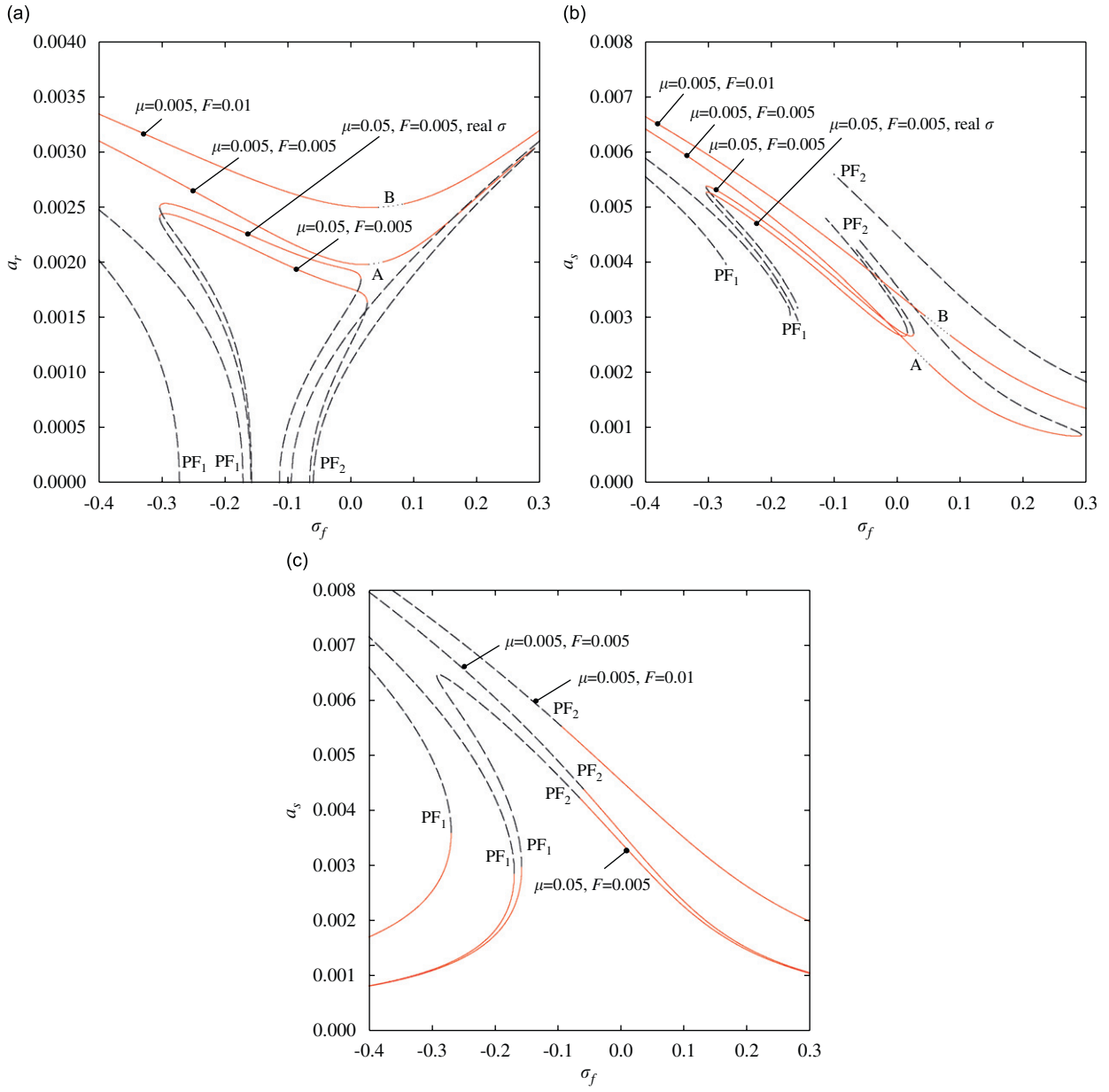

Fig. 2. MS-based frequency-response curves and bifurcations of 1:1 resonant first-crossover cable with the effect of control parameters: (a) coupled a_r, (b) coupled a_s, and (c) uncoupled a_s.

left support ($x = 0.26$) is preferably assumed as such a benchmark point in the first- and second-crossover cable analyses, respectively.

Considering the first-crossover cable with $\mu = 0.05$, $F = 0.005$ (Fig. 2c), uncoupled v displacements (Y^+, Y^-) corresponding to $\sigma_f\,(a_s) = -0.3$ (0.001094) and 0.1 (0.002249) are comparatively shown in Fig. 4a. The spatial resemblance to the primary-resonant first-symmetric mode (Fig. 1b) is apparent, and the upward–downward (e.g., mid-span) amplitude differences (drifts) due to the second-order spatial corrections of all retained (higher-order) symmetric modes [9] are observed, being enhanced with increasing a_s. As the 1:1 resonant interaction occurs (Fig. 2a and b), the coupled mixed modal v displacement (Y^+, Y^-) profiles are evidently asymmetric, with two opposite unequal curvatures, as shown in Fig. 4b ($\sigma_f = -0.1$, $F = 0.005$)

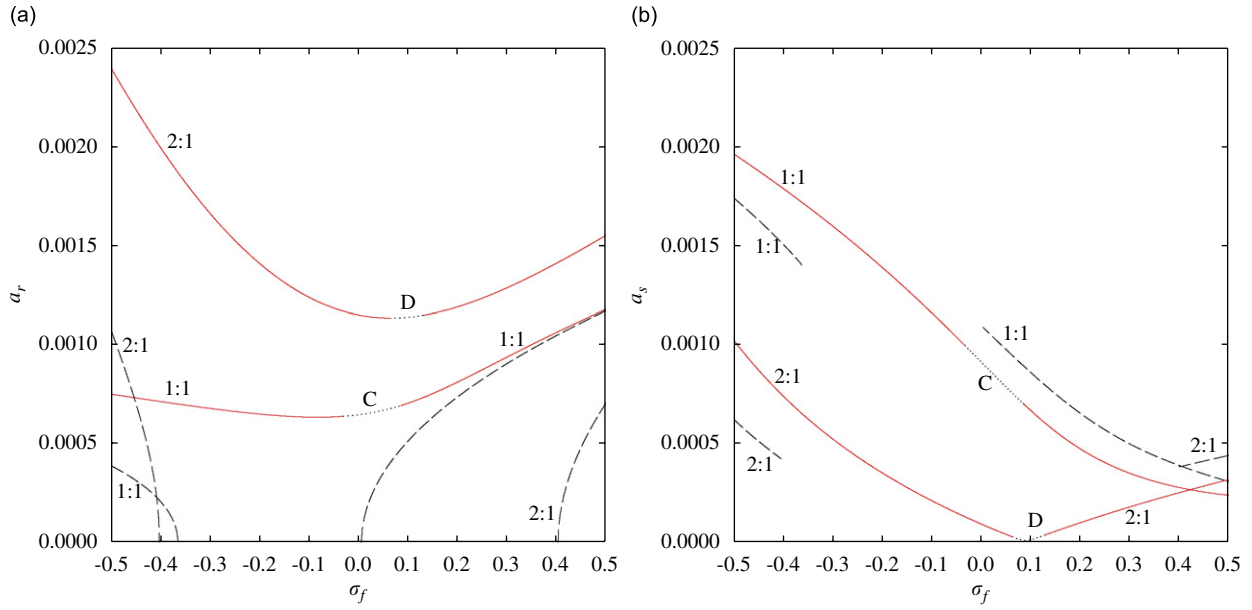

Fig. 3. MS-based frequency-response curves and bifurcations of 1:1 vs. 2:1 resonant second-crossover cable: (a) coupled a_r and (b) coupled a_s.

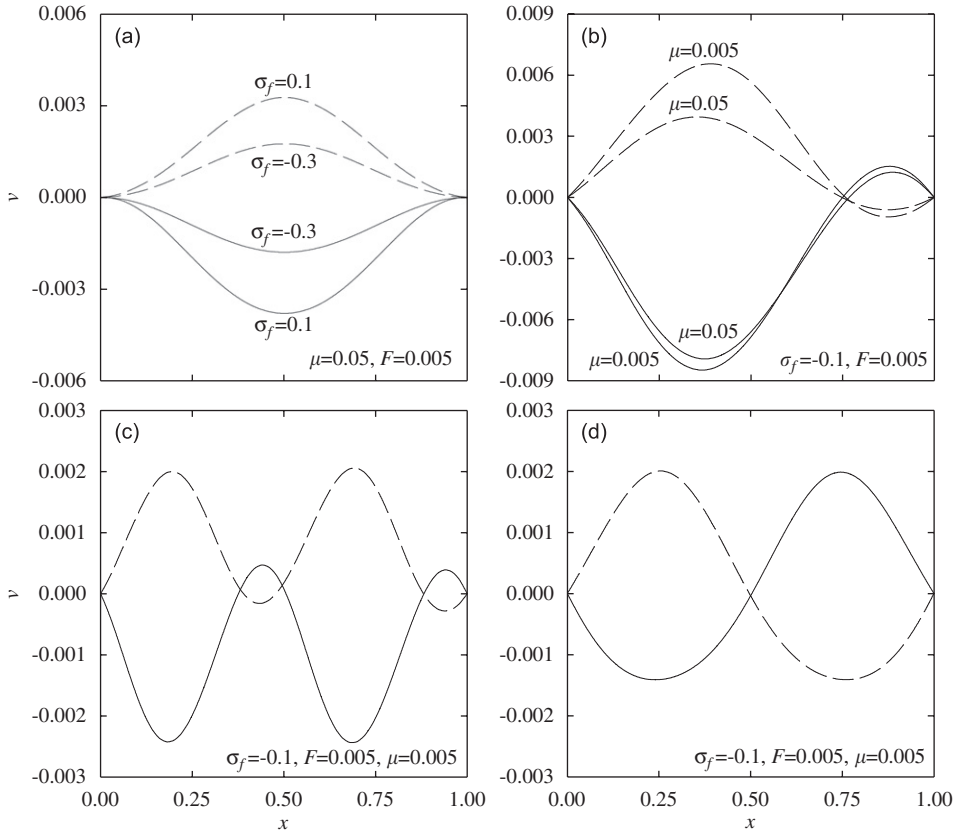

Fig. 4. MS-based spatial (Y^+, Y^-) nonlinear v dynamic configurations: (a) uncoupled and (b) coupled solutions of 1:1 resonant first-crossover cable, coupled solutions of (c) 1:1 and (d) 2:1 resonant second-crossover cable.

governing the cases (i) $\mu = 0.005$ and (ii) $\mu = 0.05$ with $(a_r,\ a_s) = (0.002186,\ 0.003842)$ and (0.001972, 0.003726), respectively. In comparison with Fig. 4a, spatial drifts in Fig. 4b are more noticeable as a result of modal interaction.

As to the second-crossover cable, it is worth distinguishing the coupled v configurations due to 1:1 resonance from those due to 2:1 resonance, by considering, for instance, $\sigma_f = -0.1$ in Fig. 3. Because of the coupled a_s (0.001163) being greater than a_r (0.000634), the 1:1 resonant (Y^+, Y^-) displacements in Fig. 4c look similar to the directly excited second symmetric mode (Fig. 1c), though being asymmetric due to the second anti-symmetric modal participation leading to some local curvature changes. On the other hand, the 2:1 resonant (Y^+, Y^-) displacements in Fig. 4d are nearly—but not completely—dominated by the driven lowest anti-symmetric mode, since a_r (0.001237) is considerably greater than a_s (0.000212). As long as the a_r amplitudes (Fig. 3a) are the most significant contributions to the coupled responses (Fig. 3), such spatial prevalence of the indirectly excited mode remains qualitatively the same, albeit sweeping σ_f towards left or right. Yet, second-order spatial corrections are observable, e.g., at quarter span, where the opposite amplitude values are unequal. In the following, the main uncoupled/coupled spatial characters of MS-based v displacements in Fig. 4 will be recognized in the numerical simulation, on the basis of their steady and maximum responses.

4. Space–time numerical simulation and validation

Depending on control parameters, overall amplitude and displacement MS predictions in Section 3 are now validated by FD simulations. After some convergence tests, it was chosen to discretize the cable through 50 intervals with $\Delta x = 0.02$ and a small time step equal to 0.0001 s. To also render the simulations stable, finite oscillating amplitudes are considered such that cables are prevented from compressive total stresses [11]. The new dimensionless time variable T, in which the original time is non-dimensionalized with respect to the forcing period, is considered. Depending on the initial u and v displacements (zero velocities), a series of space-varying time histories is carried out, capturing both transient and steady (fast and slow) dynamics over repeated cycles T. For the sake of MS–FD comparisons, histories of spatial (Y^+, Y^-) steady FD displacements, corresponding to the aforesaid benchmark points ($x = 0.5$ or 0.26) at their maxima, are determined in each (1:1 or 2:1) resonance case. In the following, reference is made to steady amplitude (Figs. 2 and 3) or spatial displacement (Fig. 4) MS results by assuming perfect internal resonance $\sigma = 0$, as σ produces a minor (negligible) quantitative (qualitative) effect (Section 3.1). Yet, whenever desirable, the actual nonlinear σ value can be evaluated a posteriori via a frequency domain analysis of the obtained FD responses (see end of Section 4.2).

4.1. Dependence of uncoupled/coupled nonlinear responses on initial conditions

As nonlinear dynamic response depends, in general, on initial conditions, it is worth examining such dependence for both uncoupled and coupled responses, by also accounting for the effect of control parameters. By way of example, the first-crossover cable is analyzed. Letting $\mu = 0.05$, $F = 0.005$, $\sigma_f = 0.1$ (Fig. 2c), Fig. 5a and b illustrate FD simulations of mid-span v amplitudes obtained with (a) zero and (b) non-zero MS-based uncoupled Y^- (solid lines) or Y^+ (dotted lines) spatial initiations (Fig. 4a). It can be seen that, irrespective of initiations and transient features, all responses reach their steady states with a comparable running time. With $\mu = 0.005$, the reduced damping role is next discussed through Fig. 5c–e based on zero initiations. With $F = 0.005$ and $\sigma_f = 0.1$, Fig. 5c exhibits a longer transient than that in Fig. 5a or b, even though all cases correspond to nearly-equal a_s MS amplitudes (Fig. 2c), which entail comparable steady FD responses. Such long transients still persist with $\sigma_f = -0.3$ (Fig. 5d), with the ensuing steady response exhibiting a smaller a_s regime in agreement with MS predictions (Fig. 2c), and they become even more remarkable, indeed also in terms of larger (transient/steady) amplitudes, in Fig. 5e when increasing the forcing to $F = 0.01$. These results show the capability of FD simulation to account for μ and F effects on transient outcomes.

Nonetheless, directly initiating the associated spatial (e.g., Y^-) uncoupled MS configuration (Fig. 5f) entails reducing significantly (approximately by half) the overall transient time with respect to that in Fig. 5e. This

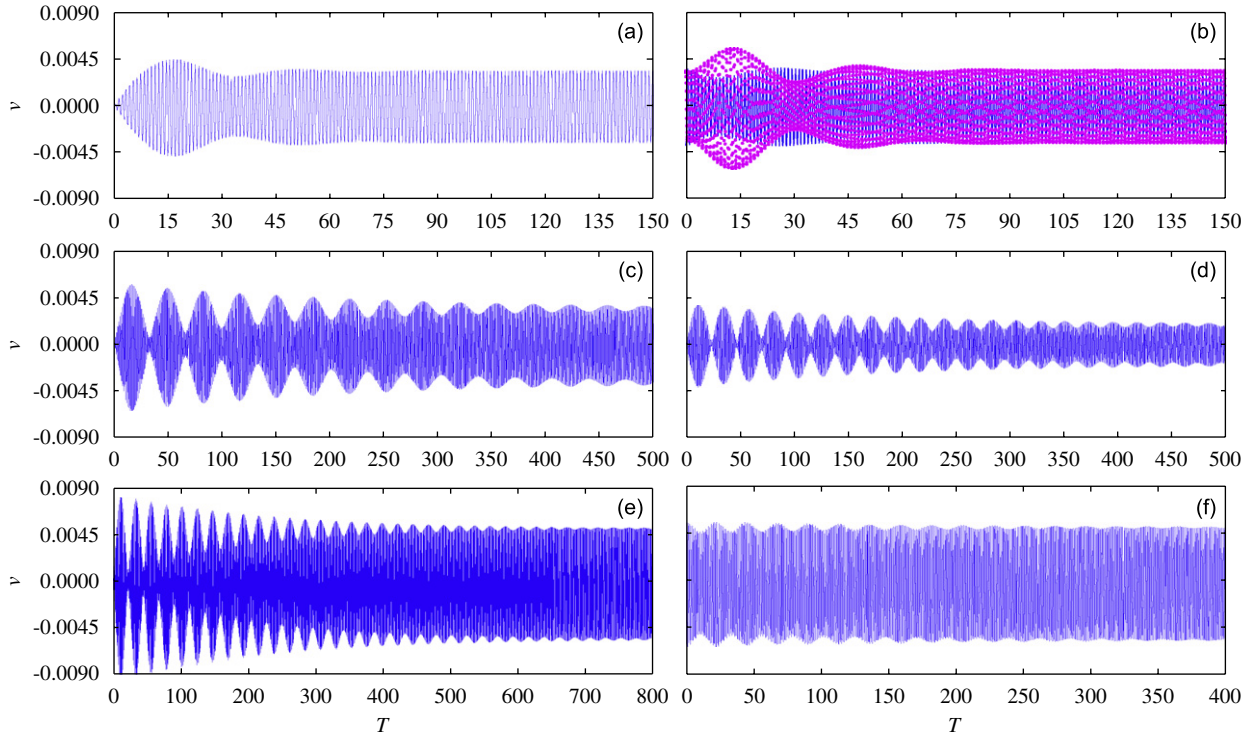

Fig. 5. FD-based nonlinear time v responses at $x = 0.5$ of 1:1 resonant first-crossover cable: (a) and (b) $\mu = 0.05$, $F = 0.005$, $\sigma_f = 0.1$ with (a) zero or (b) uncoupled MS spatial (Y^+, Y^-) initiations; (c) and (d) $\mu = 0.005$, $F = 0.005$, (c) $\sigma_f = 0.1$ or (d) $\sigma_f = -0.3$ with zero initiations; (e) and (f) $\mu = 0.005$, $F = 0.01$, $\sigma_f = 0.1$ with (e) zero or (f) uncoupled MS spatial (Y^-) initiations.

highlights that, even though both FD simulations (Fig. 5e and f) ultimately yield the same steady outputs—revealing also a slight drift due to quadratic nonlinearities (e.g., Fig. 4)—utilizing the spatial MS-based uncoupled displacements as direct initiations in FD analysis is useful for saving computational time. This is reasonable because the predicted steady MS amplitudes (Fig. 2c) actually govern the slow-varying dynamics via modulation equations. Because of small a_s, the corresponding spatial FD distributions (not displayed) of all responses in Fig. 5 show no feature of modal interaction, thus confirming the occurrence of uncoupled solutions characterized by the primary-resonant first-symmetric mode, similar to that constructed in Fig. 4a.

Depending on spatial initiations, it is now necessary to understand how responses actually evolve as the 1:1 resonant coupling comes into play. To this end, the first-crossover cable for which the MS analysis entails only stable coupled solution in Fig. 2, is again considered in Fig. 6 with $\mu = 0.005$, $F = 0.005$ and $\sigma_f = -0.1$. To discriminate spatially coupled (asymmetric) from uncoupled (symmetric) v responses (e.g., Fig. 4b vs. a) throughout the time running, FD responses at about cable quarter-span from left ($x = .2$) and right ($x = .8$) supports are comparatively recorded with black and gray lines, respectively, along with the corresponding spatial displacements during a period of peak-to-peak steady amplitudes.

First of all, zero initiations are considered and some qualitative differences between transient and steady responses are revealed in Fig. 6a. At the beginning, both quarter-span responses have equal amplitudes; thus, spatial responses are associated with the first-symmetric mode, due to the solely primary resonance. However, the spatial symmetry is destroyed at $T \approx 300$ after which the anti-symmetric mode is periodically driven into the response due to actual activation of 1:1 resonance eventually giving rise to unequal-amplitude steady responses, with the right quarter-span one becoming greater than the other. Clear combination of resonant symmetric/anti-symmetric displacements is evidenced, which entails different profiles with respect to the corresponding MS (Y^+, Y^-) ones in Fig. 4b as regards the relative phases. This may be attributed to the fact that the MS analysis relies upon constrained modal phases ensuing from the linear eigenfunctions (Fig. 1b),

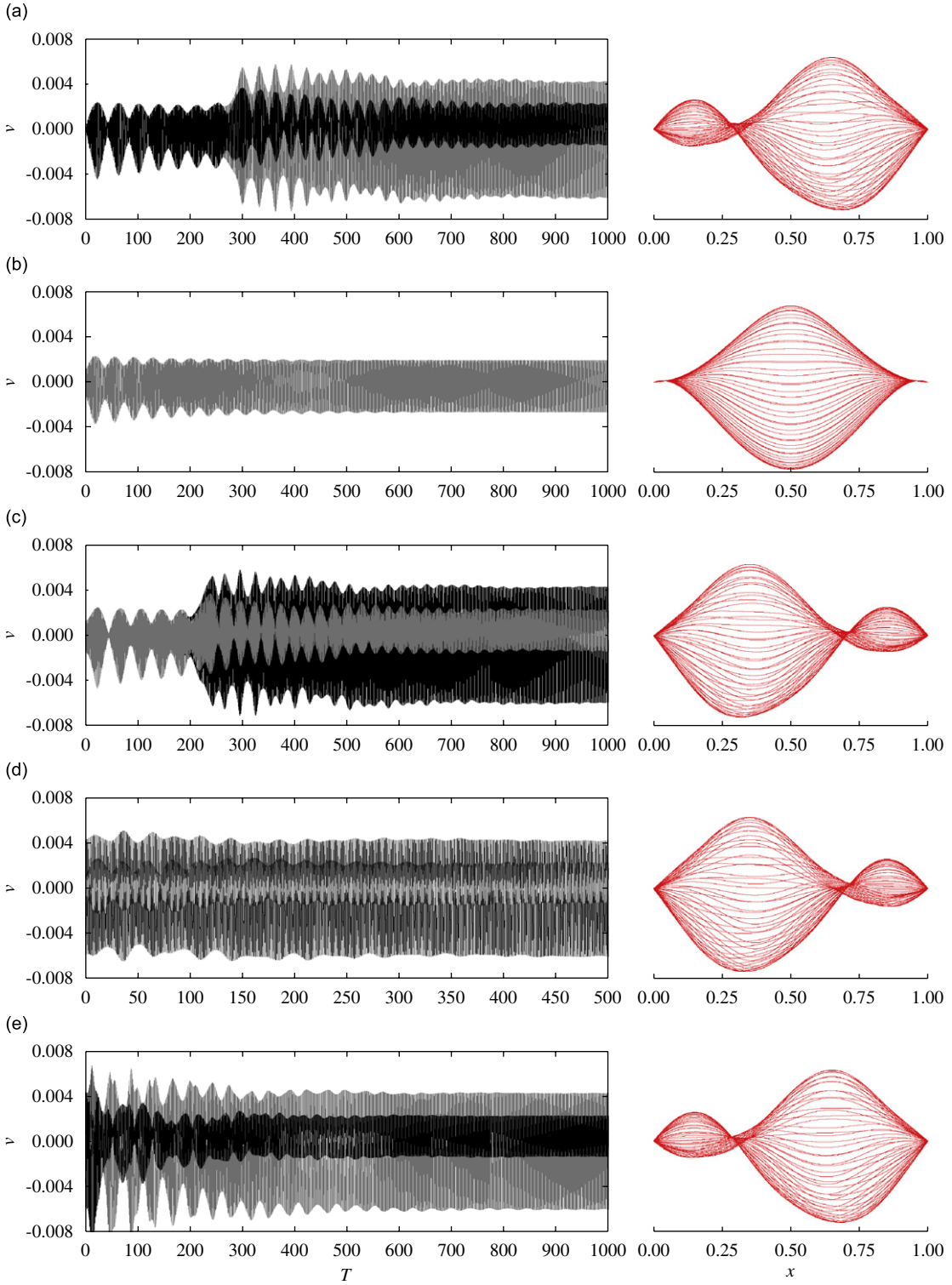

Fig. 6. FD-based nonlinear time v responses at $x = 0.2$ (black) and 0.8 (gray), and corresponding steady v displacement profiles of 1:1 resonant first-crossover cable with $\mu = 0.005$, $F = 0.005$, $\sigma_f = -0.1$: (a) zero, (b) and (c) uncoupled MS spatial (Y^-, Y^+) and (d) and (e) coupled MS spatial (Y^-, Y^+) initiations.

which affect the analytical spatial displacements, Eq. (4), whereas direct FD simulations with zero initiations are independent of such constraints.

The development of coupled from initiated uncoupled response is now discussed. Because no stable uncoupled MS solution exists at $\sigma_f = -0.1$ (Fig. 2c), spatial uncoupled MS configurations at a neighboring frequency value ($\sigma_f = 0.1$), similar to Fig. 4a, are utilized. By initiating with the phase-different Y^- and Y^+ uncoupled MS configurations, remarkably quantitative as well as qualitative differences arise between Fig. 6b and c, respectively. In particular, the responses in Fig. 6b do not signal any modal coupling feature, maintaining the symmetric displacements, and they rapidly reach steady regimes. On the contrary, Fig. 6c highlights that the initiated uncoupled responses are no longer stable after some transient periods ($T \approx 200$), where the mixed modal interaction due to 1:1 resonance comes into play, affecting the spatial transition behavior from the imposed symmetric uncoupled to steady asymmetric coupled responses. These FD results reveal how the onset of coupled responses depends on the phases of initiated uncoupled MS displacements. Yet, the left (right) quarter-span steady response in Fig. 6c is greater (smaller), thereby producing resonant profiles differing, again in terms of relative phases, from those in Fig. 6a, although both of them evidence coupled dynamics.

Not only do the spatial phases of uncoupled initiations, but also those of coupled initiations, affect the FD outcomes. By directly initiating with the phase-different Y^- vs. Y^+ coupled MS configurations at $\sigma_f = -0.1$ (i.e., Fig. 4b), relevant steady FD responses entail again meaningful phase-different coupled dynamics in Fig. 6d vs. e, even if both initiations rely on the same MS amplitude solution. In essence (Fig. 6d), initial transient periods are substantially eliminated and corresponding coupled profiles are similar to those in Fig. 6c. Conversely, longer transients are observed in Fig. 6e exhibiting also the initial phase exchange that makes the ensuing coupled profiles similar to those in Fig. 6a. Thus, depending on spatial initiations and associated phases, actual FD responses in Fig. 6 allow us to identify, regarding steady spatial displacements, three coexisting numerical solutions consisting of either one uncoupled (Fig. 6b) or two coupled (Fig. 6a and e or Fig. 6c and d) responses, in contrast with the uniquely constrained spatial MS solution of Fig. 4b. In particular, zero spatial initiation is seen to lead to the former coupled response, likely in connection with the spatial response drift towards Y^- direction observed in Fig. 4b. Towards the aim of comparing individual MS–FD spatial distributions, attention is turned to the case of spatial Y^- coupled initiations (Fig. 6d) because, besides leading to dynamic coupled profiles qualitatively resembling those predicted by the MS solution (Fig. 4b), it does not need a mammoth calculation task with respect to other initiation cases. This will be addressed in Section 4.2.

Overall, the actual existence of amplitude-steady uncoupled/coupled damped forced FD responses validates the fixed-point MS predictions based on reduced-order models. Yet, the space/time-varying FD analyses highlight the influence of spatial initiations and associated phases on the spatial numerical outcomes being actually governed by either the solely external resonance or both external/internal resonances. Meaningful transient and dynamic-instability mode-transition characteristics are revealed. Against the case of zero initiations, utilizing proper MS-based spatial configurations as FD initiations considerably reduces the computational CPU time in reaching steady-state responses. This numerical aspect appears practically advantageous when handling weakly damped multi-degree-of-freedom responses.

4.2. Role of coexisting resonant dynamics and spatial displacement comparisons

Due to coexistence of uncoupled/coupled solutions (Fig. 2), 1:1 vs. 2:1 internally resonant modal interactions (Fig. 3) and possible amplitude-modulated solutions (Figs. 2 and 3), it is worthwhile assessing the actual role of such analytically predicted coexisting dynamics—when varying control parameters—via numerical simulations based on relevant initiations. Of practical concern, overall quantitative and qualitative comparisons of MS vs. FD solutions are thoroughly made in terms of (steady state) spatial (Y^+, Y^-) v displacement distributions meaningful for reliable dynamic stress estimations (see Section 4.3).

By considering the first-crossover cable with different sets of (μ, F, σ_f), Fig. 7 compares 1:1 resonant configurations between MS (lines) and FD (circles) solutions. As anticipated in Section 4.1, all FD simulations in Fig. 7 are obtained with the fixed Y^- spatial initiation of MS coupled solution with $\mu = 0.005$, $F = 0.005$, $\sigma_f = -0.1$. Relevant to Figs. 6d and 4b, Fig. 7a provides a good qualitative and quantitative agreement of

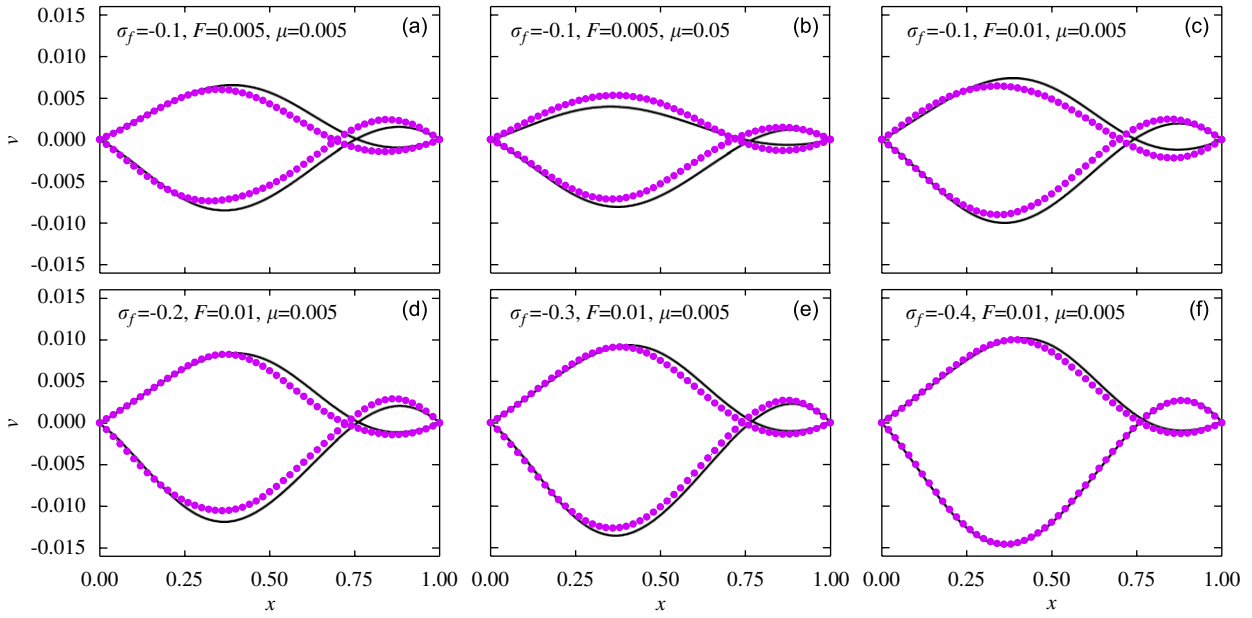

Fig. 7. A comparison of steady (Y^+, Y^-) nonlinear coupled v displacement profiles of 1:1 resonant first-crossover cable with influence of control parameters: solid lines (circles) denote MS (FD) solution.

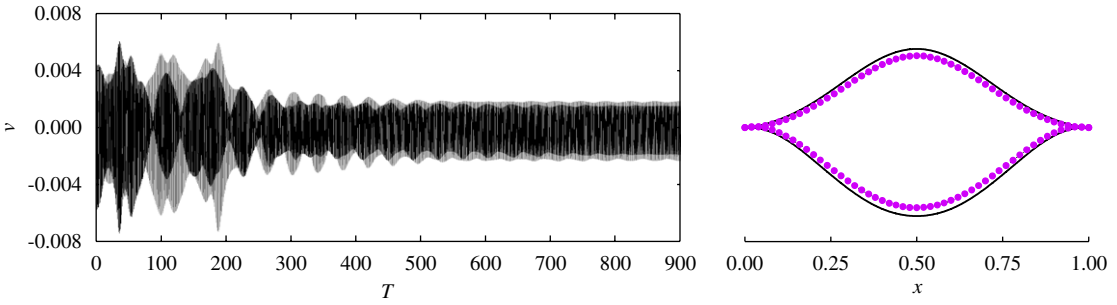

Fig. 8. FD-based nonlinear time v responses at $x = 0.2$ (black) and 0.8 (gray), and a comparison of steady (Y^+, Y^-) nonlinear uncoupled v displacement profiles of 1:1 resonant first-crossover cable with $\mu = 0.005$, $F = 0.005$, $\sigma_f = 0$: solid lines (circles) denote MS (FD) solution.

asymmetric nonlinear Y^+ and Y^- resonant profiles, in terms of both amplitudes and relative phases. This holds satisfactorily also in the case of increased $\mu = 0.05$ (Fig. 7b) or $F = 0.01$ (Fig. 7c), while keeping other parameters fixed. Then, σ_f is varied towards increasing a_r–a_s (Fig. 2a and b). It is seen that all of the FD outcomes in Fig. 7d ($\sigma_f = -0.2$), 7e ($\sigma_f = -0.3$) and 7f ($\sigma_f = -0.4$) validate the analytical MS predictions regarding the applicable range of asymptotic amplitudes. It is also worth noting that stable uncoupled MS responses, though coexisting in such σ_f range, do not play any role since coupled MS responses (Fig. 6d) are initiated in FD simulations.

The actually prevailing role played by the uncoupled responses against coupled ones is now highlighted. Indeed, when being outside the predicted range in between PF_1 and PF_2 bifurcations in Fig. 2a and b, it follows from Fig. 5b and f that steady FD responses are uncoupled when uncoupled MS solutions are initiated (Fig. 2c). However, such a persistence of spatial shape initiation does not occur any more when initiating with coupled MS solutions, as shown, e.g., in Fig. 8 with $F = 0.005$, $\mu = 0.005$ and $\sigma_f = 0$. Being the σ_f value right of PF_2 bifurcation, both quarter-span FD v responses in Fig. 8 tend, after variable amplitude transients due to asymmetric coupled initiations, to comparable values associated with spatially symmetric vibration (Y^+, Y^-) profiles (circles) typical, of course, of the first-symmetric mode and resembling very much those (solid lines) predicted by MS solution. Quantitative differences are practically less than those of coupled responses (Fig. 7),

which experience a mixed modal interaction. When being away from any modulated (periodic) solution, such circumstance occurs even if sweeping σ_f further away to the right or initiating with a_r-dominant coupled MS configurations at the associated σ_f. This predominance of uncoupled FD responses right of PF_2 bifurcation is anyhow related to MS predictions in Fig. 2, whose uncoupled a_s amplitudes (Fig. 2c) are greater than the corresponding coupled ones (Fig. 2b), implying that the primary resonance plays a greater role than the 1:1 resonance. It is the case opposite of Fig. 7, where, sweeping σ_f left of PF_2 bifurcation, coupled FD responses settle down when initiating coupled MS responses, as the predicted coupled (uncoupled) a_s are considerably greater (smaller).

Yet, by continuously sweeping σ_f farther below the left SN, such steady coupled responses in Fig. 7 do not occur anymore because of a jump phenomenon. As predicted in Fig. 2, e.g., with a fixed $F = 0.005$, the coupled MS solution shows how the cable with meaningful ($\mu = 0.05$) or small ($\mu = 0.005$) damping loses stability via SN at plausibly small ($\sigma_f \approx -0.3035$) or meaningless large ($\sigma_f \approx -30$) a_r–a_s responses, respectively. Accordingly, the FD simulations with coupled MS initiations validate ($\mu = 0.05$) or strongly revise ($\mu = 0.005$) such predictions of jump phenomena by highlighting the occurrence of steady small-amplitude uncoupled responses at $\sigma_f \approx -0.33$ in Fig. 9a ($\mu = 0.05$) and $\sigma_f \approx -0.77$ in Fig. 9b ($\mu = 0.005$).

In turn, the actual existence of nonlinear periodic response associated with a predicted Hopf bifurcation is also ascertained. By focusing on the coupled branches in Fig. 2a and b with $\mu = 0.005$ and $F = 0.01$, the MS local stability shows that two Hopf bifurcations delimit a marginal σ_f range ($\sigma_f \approx 0.0429$ and 0.0836). The FD simulations in Fig. 10a and b validate this prediction by highlighting, besides transient dynamics, the steadily amplitude-modulated responses governing the coupled u (Fig. 10a) and v (Fig. 10b) amplitudes at $\sigma_f = 0$, with assigned spatial coupled initiations as in Figs. 7 and 8. It is worth noting that the u amplitude is one order of magnitude less than the v one for the considered low-extensible cable, thus confirming through FD simulations some previous indications [9] furnished by MS. Yet, the prominent effect of u displacement in the nonlinear dynamics of highly extensible cables is dealt with in Ref. [25].

The second-crossover slacker cable is now analyzed, towards the aim of understanding—via FD simulations—whether 1:1 or 2:1 resonance activation actually predominates in the dynamic response as their independent MS solutions coexist in the whole considered σ_f range in Fig. 3, with identical $\mu = 0.005$ and $F = 0.005$. Recall also that cable node at $x = 0.26$ is assumed as the benchmark point concerning spatial (Y^+, Y^-) displacements. Following Section 4.1, a similar analysis—aimed at determining proper spatial initiations for coupled FD responses—has been performed, ending up with the choice to use, for a pertinent σ_f, spatial Y^- coupled 1:1 (like first-crossover cable) and Y^+ coupled 2:1 resonant MS displacements (e.g., Fig. 4c and d) as initiations in the relevant FD cases. Upon varying σ_f, for each spatial 1:1 or 2:1 resonant initiation, the associated steady-state FD outcomes of v amplitudes at $x = 0.26$ are comparatively zoomed in Fig. 11 with solid lines (1:1) or circles (2:1), respectively.

Starting with $\sigma_f = -0.4$, both FD simulations in Fig. 11a show qualitatively different, though quantitatively similar, steady states, regarding the relative phases, owing to different initiations. At $\sigma_f = -0.2$, the two responses coincide (Fig. 11b), with smaller amplitudes than those in Fig. 11a, as predicted in Fig. 3. To gain overall insight into global responses, the relevant (Y^+, Y^-) displacement comparisons are depicted in Fig. 11c, in which both 1:1 (solid lines) and 2:1 (circles) resonant FD simulations are plotted against MS (dashed lines)

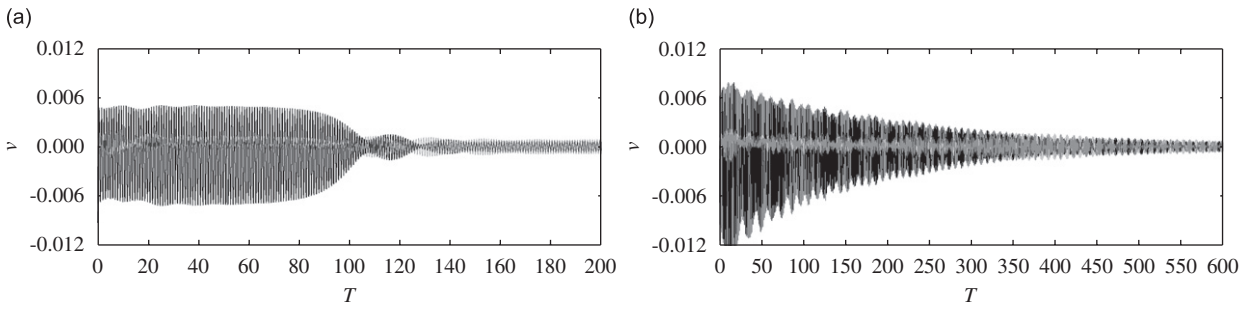

Fig. 9. FD-based nonlinear time v responses at $x = 0.2$ (black) and 0.8 (gray) of 1:1 resonant first-crossover cable below actual jump phenomenon to uncoupled response: (a) $\mu = 0.05$, $F = 0.005$ and (b) $\mu = 0.005$, $F = 0.005$.

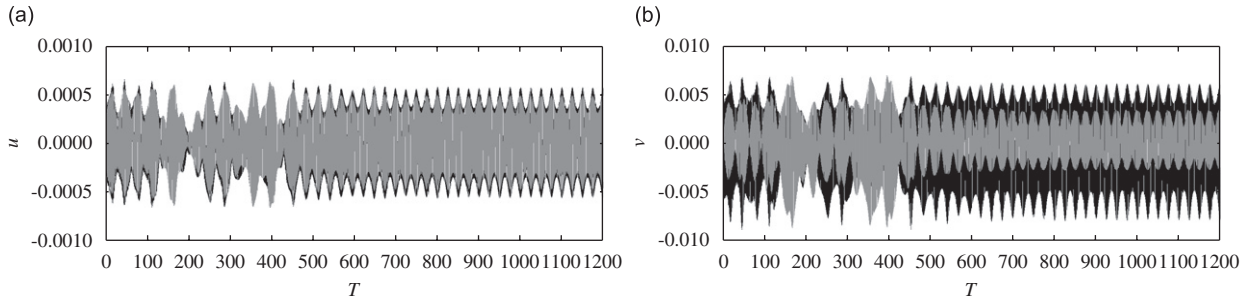

Fig. 10. FD-based nonlinear time u (a) and v (b) responses at $x = 0.2$ (black) and 0.8 (gray) of 1:1 resonant first-crossover cable showing periodically amplitude-modulated modal interactions with $\sigma_f = 0$, $\mu = 0.005$, and $F = 0.01$.

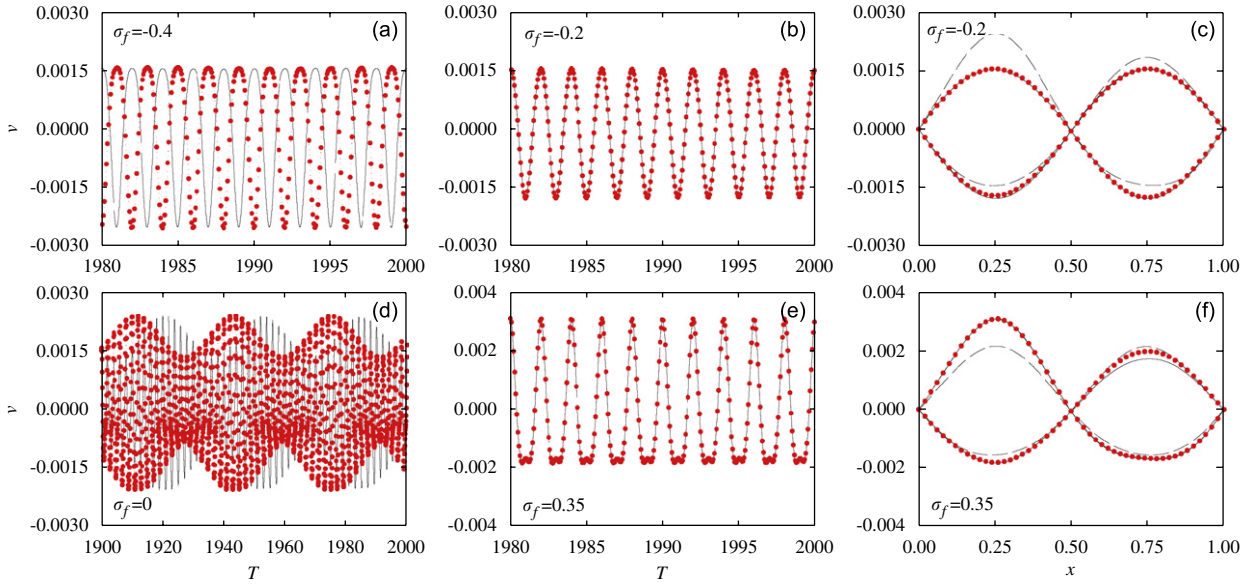

Fig. 11. FD-based nonlinear time v steady responses of second-crossover cable with $\mu = 0.005$, $F = 0.005$, (a) $\sigma_f = -0.4$, (b) $\sigma_f = -0.2$, (d) $\sigma_f = 0$, and (e) $\sigma_f = 0.35$: solid lines (circles) denote 1:1 (2:1) resonant MS-based spatial initiations, along with spatial (Y^+, Y^-) v displacement comparisons for $\sigma_f = -0.2$ (c) and $\sigma_f = 0.35$ (f): solid lines (circles) denote FD solution with 1:1 (2:1) resonant MS-based spatial initiations; dashed lines denote MS solution.

2:1 resonant results (e.g., Fig. 4d). It can be seen that, apart from a quantitative deviation of MS displacements from the other two perfectly matched FD displacements, all of them put into evidence the nearly predominating lowest anti-symmetric mode due to the major role of 2:1—against 1:1—resonance, in accordance with what observed in Fig. 3a. This highlights how the coexisting 1:1 resonance does not play any role even when directly initiating with spatial 1:1 resonant displacements. Such circumstance holds even when sweeping σ_f right of $\sigma_f = 0$ in Fig. 3, as shown in Fig. 11e ($\sigma_f = 0.35$) with the relevant displacement comparison given in Fig. 11f. Moreover, with $\sigma_f = 0$, both 1:1 and 2:1 resonant initiations in Fig. 11d end up with a beating-type phenomenon and amplitude-modulated feature due to periodical energy transfer of 2:1 resonant interaction. This validates Fig. 3 about how periodic 2:1 resonant amplitudes may originate from the nearby Hopf bifurcation at $\sigma_f = 0.123$. Overall, such numerically observed prevailing role of 2:1 over 1:1 resonance is in qualitative agreement with that observed in nonlinear undamped free planar vibrations [11], where directly initiating the second symmetric mode at second crossover entails 2:1 resonant interaction involving the first anti-symmetric mode, instead of the coexisting 1:1 resonant interaction involving the second anti-symmetric mode. With regard to CPU time, all FD simulations in Fig. 11 require a number of forcing

periods (>1500) to achieve steady responses longer than that (<1000) for lower-sagged first-crossover cable (e.g., Fig. 6).

Finally, it is certainly worth evaluating the actual internal detuning σ parameter from a transient-free FD time series since the overall discussion of interrelated FD–MS solutions is based on $\sigma = 0$. As an example, a Fourier-based analysis of the two simulations in Fig. 11a is performed, and the results of 1:1 and 2:1 resonant initiations are plotted in Fig. 12a and b, respectively. Remarkably, both responses highlight two major peaks, with a_r being greater than a_s, which is in good accordance with the 2:1 resonant MS prediction in Fig. 3 for $\sigma_f = -0.4$. The corresponding two nonlinear frequency values are the same in both plots, i.e., 0.165 and 0.328 Hz, thus providing a nearly perfectly tuned 2:1 frequency ratio. Apart from confirming the actually predominant role of 2:1 resonance at second crossover, relying upon $\sigma = 0$ in MS solutions appears reliable for MS–FD comparisons.

4.3. Discussion on approximate/exact and planar/non-planar cable modeling

For the sake of completeness, straightforward FD analyses of more realistic cable models are now addressed shortly. Based on the same assigned control parameters and initial conditions, attention is paid to highlighting (i) the validity of approximate PDEs (1) and (2) vs. the exact ones [11] for planar motion, and (ii) the limitation of the approximate planar (2-D) modeling (herein considered) vs. the associated non-planar (3-D) one [7].

Regarding the first issue, the FD responses of the approximate PDEs are compared with those of the exact PDEs, which hold for also a larger amplitude range and a larger sagged cable. Comparisons for both uncoupled and coupled (constant- or varying-amplitude) solutions are made in terms of induced nonlinear dynamic tensions whose strains are spanwise non-uniform [9], thus being of remarkable engineering significance. By considering the first-crossover cable, the benchmarking (mid-span) responses of dynamic tension τ, normalized with respect to the maximum static tension, are compared in Fig. 13, whose left (right) column represents approximate (exact) PDEs' outcomes. Various cases of 1:1 resonant steady or modulated responses are considered, with Fig. 13a, c, e (b, d, f), corresponding to Fig. 2 ($\mu = 0.005$, $F = 0.01$, $\sigma_f = 0.1$), Figs. 7f and 10b, respectively. The available maximum/minimum τ values of fixed-point MS solutions are also reported in Fig. 13a and c with horizontal lines. Interestingly, Fig. 13 highlights overall qualitative as well as quantitative agreements for both steadily constant-amplitude (Fig. 13a–d) and varying-amplitude (Fig. 13e and f) τ responses between MS-approximate, FD-approximate and FD-exact modeling, along with the compatibility of FD transient periods and features. Thus, for finite-amplitude vibrations of small-sagged cable, the MS–FD nonlinear tension responses are both valid and the associated approximate PDEs (1) and (2) can be used reliably.

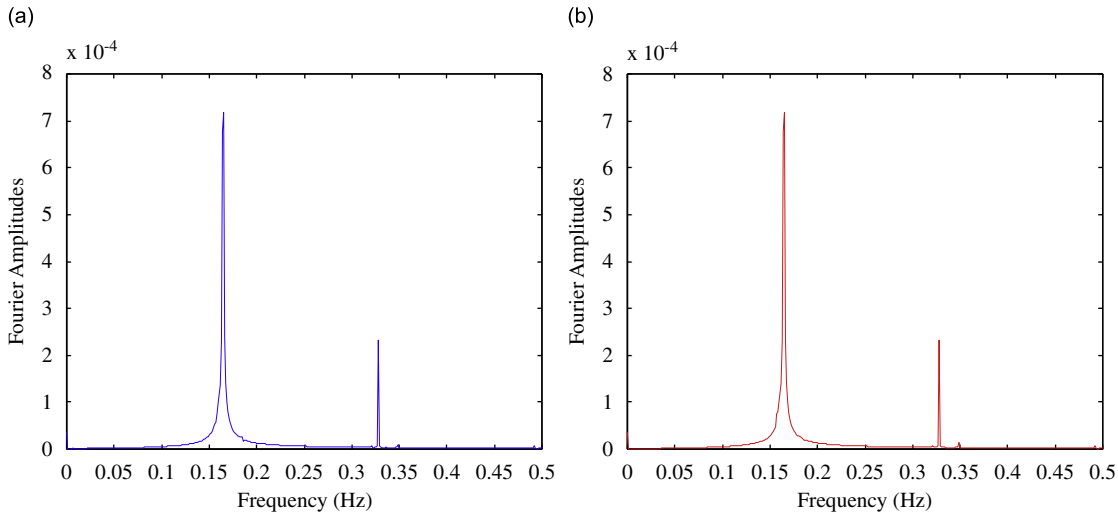

Fig. 12. Fourier-based frequency analysis of Fig. 11a: (a) 1:1 and (b) 2:1 resonant MS-based spatial initiations.

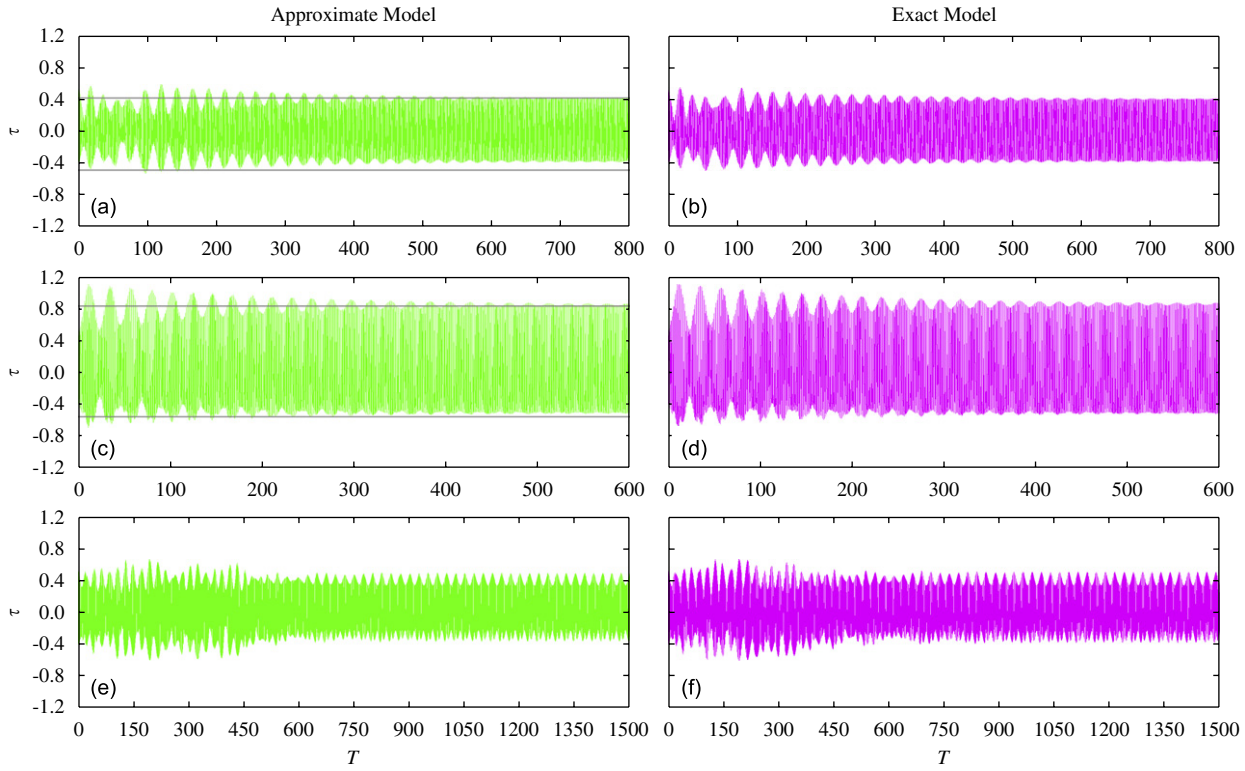

Fig. 13. FD simulation of cable nonlinear dynamic tension at mid-span based on approximate (a, c and e) vs. exact (b, d and f) planar modeling: (a, b), (c, d) and (e, f) correspond to Fig. 2 ($\mu = 0.005$, $F = 0.01$,$\sigma_f = 0.1$), Figs. 7f and 10b, respectively; horizontal lines in (a, c) denote corresponding maximum/minimum MS results.

Regarding the second issue, it is well known [1] that multiple internal resonances involving also out-of-plane (w) modes and planar vs. non-planar response scenarios [3,4] differing from those predicted in Figs. 2 and 3, do exist at crossovers. Investigating them systematically in the analytical–numerical comparison perspective herein pursued would require extensive and heavy MS–FD analyses. We just limit ourselves to reconsidering both crossover cables to show how the modulated planar responses obtained with the 2-D model turn into steady non-planar responses when correctly considering the associated 3-D model [7] with the same planar/non-planar damping ($\mu = 0.005$). Focusing on $\sigma_f = 0$, whose periodically amplitude-modulated FD v responses based on planar model are given in Figs. 10b and 11d, the corresponding FD v ($x = 0.50$) and w ($x = 0.26$) responses based on non-planar model are plotted in Fig. 14a, d and b, e, for first- and second-crossover cables, respectively. It can be seen that in both responses, after some transients, the initiated planar amplitudes decrease up to low values, whereas substantial non-planar amplitudes are born from trivial values, exhibit some transients and then become ultimately steady. Correspondingly, the spatial displacement profiles visualized in Fig. 14c and f show the character of lowest symmetric (Fig. 14c) and anti-symmetric (Fig. 14f) out-of-plane modes, the coexisting non-planar 2:1 resonance actually predominating against the planar 1:1/2:1 resonances at first/second crossovers, respectively, and entailing overall regularization of cable responses. Thus, the constrained planar model can be inadequate for such a systematic response analysis, and it is definitely advised to use the complete 3-D model for capturing, analytically and numerically, the actual non-planar resonant dynamics.

5. Summary and concluding remarks

Space–time FD simulation of the PDEs governing geometrically nonlinear forced dynamics of suspended cables under primary external and 1:1 or 2:1 internal resonances has been carried out, in order to validate the

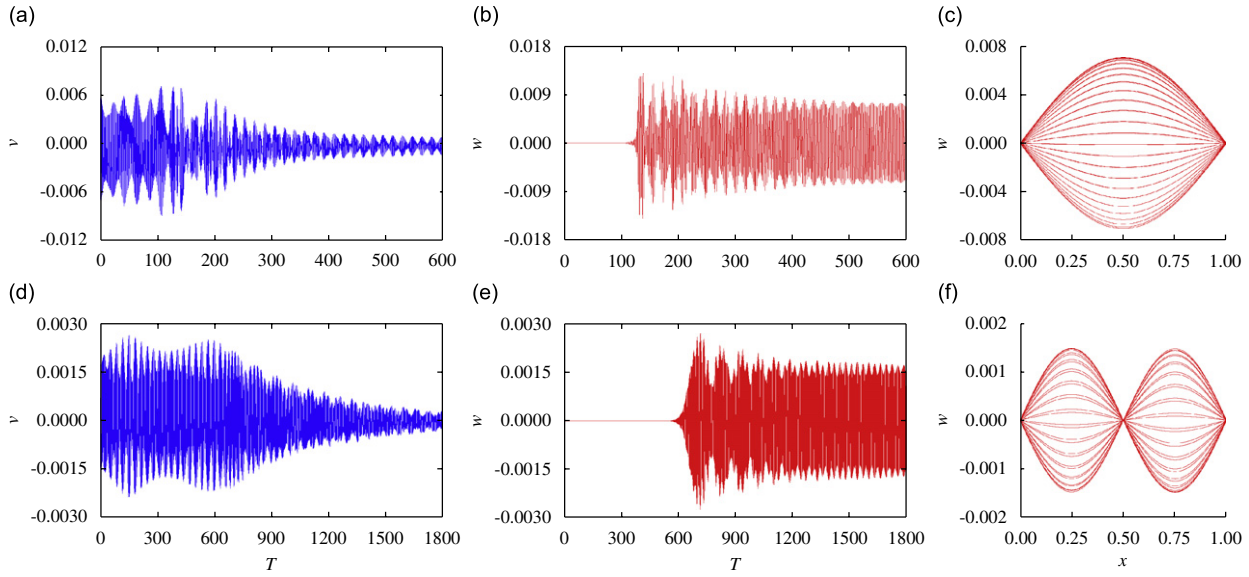

Fig. 14. FD simulation of cable v and w responses at mid-span (a, b) and quarter-span (d, e) based on approximate 3-D modeling: (a, b) and (d, e) correspond to first and second-crossover cables with symmetric (c) and anti-symmetric (f) out-of-plane vibration profiles, respectively.

MS-based analytical predictions of the associated finite-dimensional ODEs. Different sagged horizontal cables at the first two crossovers involving mixed symmetric/anti-symmetric modal interactions have been analyzed, by relying on the approximate, kinematically non-condensed, planar modeling. With weakly quadratic/cubic nonlinearities and multiple modal contributions, local scenarios of stable/unstable and uncoupled/coupled MS solutions have been evaluated by means of frequency-response curves and bifurcations, accounting for also the influence of other control parameters. Towards the aim of interrelating analytical and numerical solutions, corresponding amplitude-dependent, damped, forced, resonant MS displacements have been constructed and further utilized, as spatial initiations, in the FD simulations which allow us to capture both fast and slow dynamics.

Depending on system control parameters and spatial initiations, space–time-varying FD results reveal the actual existence of steady-state uncoupled (symmetric) vs. coupled (mixed) amplitude (displacement) MS solutions, along with meaningful transient evolution and dynamic-instability, mode-transition, characteristics. As regards the computational CPU time effort, directly initiating with proper MS-based spatial configurations makes the steady-state FD responses accessible with fewer transient periods than those necessary with conventional zero initiations. This allows undertaking large parametrical studies, which are needed for practical applications. The observed variability of spatial numerical outcomes—highlighting the actual predominance of solely external or combined external/internal resonances—mainly depends on whether the initiated displacements/phases are zero, uncoupled or coupled, in contrast with the analytical solutions whose spatial distributions and relative phases are constrained to pertinent eigenfunctions and modulation equations, respectively.

With reference to a cable benchmarking point, comparisons of uncoupled/coupled (downward/upward) spatial MS–FD displacements highlight quantitative as well as qualitative agreement of multi-degree-of-freedom responses. Thus, overall numerical results thoroughly validate the analytical predictions. Apart from the limitation of the considered 2-D cable modeling, substantial parametric findings enable us to precisely identify the role of coexisting/competing (uncoupled vs. coupled) resonant dynamics, the actual jump phenomena with the relevant amplitude range, the predominant 2:1 vs. 1:1 (as well as non-planar vs. planar) internal resonance, the periodically amplitude-modulated coupled responses, the actual nonlinear frequencies, and the validity—through nonlinear dynamic tension comparisons—of the approximate ODEs/PDEs, against the exact PDEs, for small-sagged cables.

Finally, it is worth emphasizing that, by accounting for the multi-dimensional responses, space–time numerical simulation and validation of analytical predictions are of the utmost importance for engineering

design and practice. Besides systematically complementing the analytically disclosed dynamics, numerical achievements furnish improved understanding of the basic dynamic mechanisms, along with valuable information about the possible prevalence of actually coexisting phenomena. It is felt that the present analyses may pave a complete methodological way for accomplishing a 3-D investigation of arbitrarily-inclined cable nonlinear forced vibrations aimed at a comprehensive description of out-of-plane/in-plane responses.

Acknowledgements

The first author wishes to acknowledge a Postdoctoral Fellowship from SAPIENZA University of Rome, Italy.

References

[1] G. Rega, Nonlinear dynamics of suspended cables, part I: modeling and analysis; part II: deterministic phenomena, *ASME Applied Mechanics Reviews* 57 (2004) 443–514.
[2] M. Pakdemirli, S.A. Nayfeh, A.H. Nayfeh, Analysis of one-to-one autoparametric resonance in cables-discretization vs. direct treatment, *Nonlinear Dynamics* 8 (1995) 65–83.
[3] G. Rega, W. Lacarbonara, A.H. Nayfeh, C.M. Chin, Multiple resonances in suspended cables: direct vs. reduced-order models, *International Journal of Non-linear Mechanics* 34 (1999) 901–924.
[4] A.H. Nayfeh, H.N. Arafat, C.M. Chin, W. Lacarbonara, Multimode interactions in suspended cables, *Journal of Vibration and Control* 8 (2002) 337–387.
[5] H.N. Arafat, A.H. Nayfeh, Non-linear responses of suspended cables to primary resonance excitations, *Journal of Sound and Vibration* 266 (2003) 325–354.
[6] W. Lacarbonara, G. Rega, A.H. Nayfeh, Resonant nonlinear normal modes, part I: analytical treatment for structural one-dimensional systems, *International Journal of Non-linear Mechanics* 38 (2003) 851–872.
[7] N. Srinil, G. Rega, S. Chucheepsakul, Two-to-one resonant multi-modal dynamics of horizontal/inclined cables, part I: theoretical formulation and model validation, *Nonlinear Dynamics* 48 (2007) 231–252.
[8] N. Srinil, G. Rega, Two-to-one resonant multi-modal dynamics of horizontal/inclined cables, part II: internal resonance activation, reduced-order models and nonlinear normal modes, *Nonlinear Dynamics* 48 (2007) 253–274.
[9] N. Srinil, G. Rega, The effects of kinematic condensation on internally resonant forced vibrations of shallow horizontal cables, *International Journal of Non-linear Mechanics* 42 (2007) 180–195.
[10] N. Srinil, G. Rega, S. Chucheepsakul, Large amplitude three-dimensional free vibrations of inclined sagged elastic cables, *Nonlinear Dynamics* 33 (2003) 129–154.
[11] N. Srinil, G. Rega, S. Chucheepsakul, Three-dimensional nonlinear coupling and dynamic tension in the large amplitude free vibrations of arbitrarily sagged cables, *Journal of Sound and Vibration* 269 (2004) 823–852.
[12] Y.Q. Ni, W.J. Lou, J.M. Ko, A hybrid pseudo-force/Laplace transform method for non-linear transient response of a suspended cable, *Journal of Sound and Vibration* 238 (2000) 189–214.
[13] A.A. Tjavaras, Q. Zhu, Y. Liu, M.S. Triantafyllou, D.K.P. Yue, The mechanics of highly-extensible cables, *Journal of Sound and Vibration* 213 (1998) 709–737.
[14] C.G. Koh, Y. Rong, Dynamic analysis of large displacement cable motion with experimental verification, *Journal of Sound and Vibration* 272 (2004) 187–206.
[15] Q. Zhou, S.R.K. Nielsen, W.L. Qu, Semi-active control of three-dimensional vibrations of an inclined sag cable with magnetorheological dampers, *Journal of Sound and Vibration* 296 (2006) 1–22.
[16] N.S. Abhyankar, E.K. Hall, S.V. Hanagud, Chaotic vibrations of beams: numerical solution of partial differential equations, *ASME Journal of Applied Mechanics* 60 (1993) 167–173.
[17] S. Essebier, G. Baker, Computational techniques for nonlinear dynamics of continuous systems, *ASCE Journal of Engineering Mechanics* 121 (1995) 1193–1999.
[18] A. Abe, On non-linear vibration analyses of continuous systems with quadratic and cubic non-linearities, *International Journal of Non-linear Mechanics* 41 (2006) 873–879.
[19] V. Gattulli, L. Martinelli, F. Perotti, F. Vestroni, Nonlinear oscillations of cables under harmonic loading using analytical and finite element models, *Computer Methods in Applied Mechanics and Engineering* 193 (2004) 69–85.
[20] H.M. Irvine, *Cable Structures*, MIT Press, Cambridge, MA, 1981.
[21] G. Rega, N. Srinil, Nonlinear hybrid-mode resonant forced oscillations of sagged inclined cables at avoidances, *ASME Journal of Computational and Nonlinear Dynamics* 2 (2007) 324–336.
[22] W.F. Ames, *Numerical Methods for Partial Differential Equations*, Academic Press, New York, 1977.
[23] W.L. Wood, *Practical Time-Stepping Schemes*, Oxford University Press, New York, 1990.
[24] R. Seydel, *Practical Bifurcation and Stability Analysis*, Springer, New York, 1994.
[25] N. Srinil, G. Rega, Nonlinear longitudinal/transversal modal interactions in highly extensible suspended cables, *Journal of Sound and Vibration* 310 (2008) 230–242.